BMC Chemistry

RESEARCH

Open Access

Anchoring of 2D layered materials of $Ge_5Si_5O_{20}$ for (Li/Na/K)-(Rb/Cs) batteries towards Eco-friendly energy storage

Fatemeh Mollaamin[1*]

Abstract

In this investigation, alkali metals including lithium (Li), sodium (Na), potassium (K), rubidium (Rb) and cesium (Cs) have been served as hybrid materials for batteries cells. A vast study on H-capture by "LiRb ($Ge_5Si_5O_{20}$), LiCs($Ge_5Si_5O_{20}$), NaRb($Ge_5Si_5O_{20}$), NaCs($Ge_5Si_5O_{20}$), KRb($Ge_5Si_5O_{20}$), KCs($Ge_5Si_5O_{20}$)" was probed using computational approaches due to density state analysis of charge density differences, total density of states, projected density of states, overlap projected density of states, and localized orbital locator for hydrogenated hybrid clusters of "LiRb($Ge_5Si_5O_{20}$)–$2H_2$, LiCs($Ge_5Si_5O_{20}$)–$2H_2$, NaRb($Ge_5Si_5O_{20}$)–$2H_2$, NaCs($Ge_5Si_5O_{20}$)–$2H_2$, KRb($Ge_5Si_5O_{20}$)–$2H_2$, KCs($Ge_5Si_5O_{20}$)–$2H_2$". As the benefits of "lithium, sodium or potassium" over "Ge/Si" possess its higher electron and "hole motion", permitting "Li, Na, K" devices to operate at higher frequencies than "Ge/Si" devices. Regarding optimized energy, KRb($Ge_5Si_5O_{20}$), KRb($Ge_5Si_5O_{20}$)–$2H_2$, KCs($Ge_5Si_5O_{20}$), and KCs($Ge_5Si_5O_{20}$)–$2H_2$ heteroclusters have shown more stability than LiRb($Ge_5Si_5O_{20}$), LiRb($Ge_5Si_5O_{20}$)–$2H_2$, LiCs($Ge_5Si_5O_{20}$), LiCs($Ge_5Si_5O_{20}$)–$2H_2$, NaRb($Ge_5Si_5O_{20}$), NaRb($Ge_5Si_5O_{20}$) – $2H_2$, NaCs($Ge_5Si_5O_{20}$), NaCs($Ge_5Si_5O_{20}$)–$2H_2$ heteroclusters. In this research, hydrogen energy sources on functionalized 2D materials by metals have been shown as promising alternatives for clean energy systems. In a particular way, we have demonstrated here that ($Ge_5Si_5O_{20}$) weakly adsorbs H_2. At the same time, the Li/Na/K decoration significantly enhances the H_2 interaction, accommodating to H_2 molecules by a stronger physisorption. Doping Rb or Sc on $Ge_5Si_5O_{20}$ can increase battery capacity through LiRb ($Ge_5Si_5O_{20}$), LiCs($Ge_5Si_5O_{20}$), NaRb($Ge_5Si_5O_{20}$), NaCs($Ge_5Si_5O_{20}$), KRb($Ge_5Si_5O_{20}$), KCs($Ge_5Si_5O_{20}$) nanoclusters for hydrogen adsorption process and could improve the rate performances by enhancing electrical conductivity. A small portion of "Rb or Cs" entered the "Ge–Si" layer to replace the Li, Na or K sites might improve the structural stability of the electrode material at high multiplicity, thereby improving the capacity retention rate. Among these, LiRb ($Ge_5Si_5O_{20}$), NaRb($Ge_5Si_5O_{20}$) and KRb($Ge_5Si_5O_{20}$) pretend to show the most hope in terms of "Rb" doping which can augment the capacity owing to higher surface capacitive impacts.To be specific, a scalable method is developed to fabricate the nanocomposite which acts as a simulated anode for Li-ion intercalation and subsequent Li alkali metal (Na, K/Rb, Cs) alloys owing to enhanced lithiophilicity and sufficient ion-conducting pathways.

Keywords Energy storage, Alkali metal-ion battery, density of states, Charge distribution, Materials modeling, Hydrogen adsorption

*Correspondence:
Fatemeh Mollaamin
fmollaamin@kastamonu.edu.tr
[1]Department of Biomedical Engineering, Faculty of Engineering and Architecture, Kastamonu University, Kastamonu 37150, Turkey

Introduction

Sodium/potassium-ion can be the prominent chemistry substitution applicant for LIBs [1–6]. The potassium-ion has certain privileges over analogous Li-ion like the battery cell architecture is plain, and both the construction approaches and the material are not expensive. The major benefit is the high amount and light price of K in evaluation with Li, which makes potassium batteries an engaged replacement for big size battery cells like indoor energy-saving and electric devices. Further privilege of a K-ion battery cell over a Li-ion one is efficiently charging in a short time [7–13].

Lately, the carbide hybrid nanomaterils of "Si-, Ge-, Sn " have been proposed as occupied "H_2-capture" substances [14–16]. Whereas the polarizability of Si is more than C atom, it is assumed that "Si–C/Si nanosurface" may append to compositions more intensely in hybrid to the pure C-nanostructures [17–19]. The previous investigations of energy-saving devices through H-adsorption have been tailored owing to "DFT calculations" with a semiconductor group of "Si/Ge/Sn/Pb nano-carbides" [20], "Mg-Al nanoalloy" [21] and "Al/C/ Si doping of BN nanocomposite" [22].

Nanomaterials with notable structures detect undertaking demands in the field of electrocatalysis, fuel cells, and energy-saving [23]. The ressarches have evaluated the performance of MB_4 (M = Cr, Mo, and W) monolayer MBenes as an anode material for calcium ion batteries which can be a suitable alternative to Li-ion batteries (LIBs) using density functional theory method [24].

Furthermore, it was examined the viability of 2D CrB_4 and MoB_4 monolayers as optimal anode-materials for Li/Na/K ion batteries using first-principles DFT calculations. Preliminary investigations showed that both materials exhibited thermodynamic, structural, and mechanical stability. We found that a strongly negative adsorption energy can help in stabilizing the adsorption of metal-ions on materials surface instead of clustering, that ensures metal-ion-batteries stability [25].

The apparent effect of germanium coverage on silicon monohydride desorption kinetics was evaluated based on their ability to fit temperature-programmed desorption data. Then, an evaluation of the physical consistency of the estimated kinetic constants, and a comparison with the effects of other atomic impurities on hydrogen desorption from silicon (100) were accomplished [26].

Although Ge may modify the energetics of the interaction of hydrogen and silicon, it is concluded that such an effect alone is insufficient to describe the shift and broadening of the feature, while the GeH intermediate model succeeds, even in the absence of any such effect [26].

Moreover, the influence of germanium atoms upon molecular hydrogen desorption energetics using density functional cluster calculations was studied. A three-dimer cluster is used to hybrid model. The relative stabilities of the various monohydride and clean surface configurations are computed. It was also computed the energy barriers for desorption from silicon, germanium, and mixed dimers with various neighboring configurations of silicon and germanium atoms. Their results indicated that there are two desorption channels from mixed dimers, one with an energy barrier close to that for desorption from germanium dimers and one with an energy barrier close to that for desorption from silicon dimers [20, 27].

This investigation wants to delve into the feasibility of "LiRb ($Ge_5Si_5O_{20}$), LiCs($Ge_5Si_5O_{20}$), NaRb($Ge_5Si_5O_{20}$), NaCs($Ge_5Si_5O_{20}$), KRb($Ge_5Si_5O_{20}$), KCs($Ge_5Si_5O_{20}$)" nanoclusters for H-storage. Therefore, it was analyzed the physico-chemical properties of mentioned heteroclusters and hydrogenated nanoclusters of "LiRb($Ge_5Si_5O_{20}$)–$2H_2$, LiCs($Ge_5Si_5O_{20}$)–$2H_2$, NaRb($Ge_5Si_5O_{20}$)–$2H_2$, NaCs($Ge_5Si_5O_{20}$)–$2H_2$, KRb($Ge_5Si_5O_{20}$)–$2H_2$, KCs($Ge_5Si_5O_{20}$)–$2H_2$".

This article aims to systematically investigate the key applications of theoretical calculations in energy storage devices, with a particular focus on the research progress of cathode materials and anode materials and analyse how these heteroclusters can better elucidate the actual performance of materials and anticipate the challenges and opportunities that may arise in future development. Subsequently, the recent research progress on the application of Na, K/Rb, Cs in each component of the LB is summarized, aiming to understand the hybrid forms of alkali metals and their potential for use in LB materials. Here, the aim is to provide a clear insight on the study of hybrid battery cells in energy storage materials and contribute to the promotion of further research in this area. Due to the unique structural advantages of 2D materials, these versatile 2D electrode materials have shown stable potential for hydrogen adsorption and energy storage.

Materials and methods

Theoretical calculations have become essential tools for a comprehensive understanding of the microscopic mechanisms in energy storage materials, particularly in charge density variations and electron transport characteristics behaviors in electrode materials. In our research, the calculations have been done by CAM–B3LYP–D3 level of theory. A new hybrid exchange–correlation functional named Coulomb-attenuating method- (Becke, 3-parameter, Lee-Yang-Parr) (CAM-B3LYP) is proposed. It combines the hybrid qualities of B3LYP and the long-range correction. Dispersion forces were considered under the DFT-D3 method of Grimme with Becke–Johnson damping [28]. Calculations with spin polarization were performed within the density functional theory (DFT). The exchange correlation potentials were treated using

the Perdew–Burke–Ernzerhof (PBE) parameterization within the general gradient approximation (GGA) [28].

Figure1 has shown alkali metals-based nanoclusters of "LiRb ($Ge_5Si_5O_{20}$), LiCs($Ge_5Si_5O_{20}$), NaRb($Ge_5Si_5O_{20}$), NaCs($Ge_5Si_5O_{20}$), KRb($Ge_5Si_5O_{20}$), KCs($Ge_5Si_5O_{20}$) " which can enhance the H-storage in battery cells, transistors or other semiconducting devices. In this investigation, the computations have been launched by Coulomb-attenuating method–(Becke, 3-parameter, Lee-Yang-Parr) [CAM–B3LYP–D3] level of theory. Figure 1 indicates the status of "H_2-capture" by "LiRb ($Ge_5Si_5O_{20}$), LiCs($Ge_5Si_5O_{20}$), NaRb($Ge_5Si_5O_{20}$), NaCs($Ge_5Si_5O_{20}$), KRb($Ge_5Si_5O_{20}$), KCs($Ge_5Si_5O_{20}$)" nanoclusters and hydrogen-adsorbed nanoclusters of "LiRb($Ge_5Si_5O_{20}$)–$2H_2$, LiCs($Ge_5Si_5O_{20}$)–$2H_2$, NaRb($Ge_5Si_5O_{20}$)–$2H_2$, NaCs($Ge_5Si_5O_{20}$)–$2H_2$, KRb($Ge_5Si_5O_{20}$)–$2H_2$, KCs($Ge_5Si_5O_{20}$)–$2H_2$".

The analysis of "Bader charge" parameter [29–33] has been illustrated pending H_2-capture by "LiRb($Ge_5Si_5O_{20}$)–$2H_2$, LiCs($Ge_5Si_5O_{20}$)–$2H_2$, NaRb($Ge_5Si_5O_{20}$)–$2H_2$, NaCs($Ge_5Si_5O_{20}$)–$2H_2$, KRb($Ge_5Si_5O_{20}$)–$2H_2$, KCs($Ge_5Si_5O_{20}$)–$2H_2$" hybrid clusters (Fig. 1) due to "Gaussian 16 revision C.01" computational software [34] and "GaussView 6.1" graphical program [35]. The applied basis sets for theoretical calculations of H_2-capture by "LiRb ($Ge_5Si_5O_{20}$), LiCs($Ge_5Si_5O_{20}$), NaRb($Ge_5Si_5O_{20}$), NaCs($Ge_5Si_5O_{20}$), KRb($Ge_5Si_5O_{20}$), KCs($Ge_5Si_5O_{20}$)" has been supported by "LANL2DZ and 6–311 + G (d, p)". The electronegativity, local dipole, and charge transfer are proposed to reveal the doping sites. Li, Na, K bond chemistry further deepens the understanding to exhibit the best charge transfer among single-doped and co-doped atoms, respectively. The excellent charge transfer achieved by Rb, Cs-doping $Ge_5Si_5O_{20}$ is further validated by Li, Na, K nucleation overpotential measurement. This work uncovers the charge transfer of heteroatom-doped $Ge_5Si_5O_{20}$ and affords mechanistic guidance to Li, Na, K metal anode frameworks for safe rechargeable batteries.

Results and discussion

Charge density differences analysis

In Fig. 2a–f, "charge density differences (CDD)" [36] has been shown for "LiRb ($Ge_5Si_5O_{20}$), LiCs($Ge_5Si_5O_{20}$), NaRb($Ge_5Si_5O_{20}$), NaCs($Ge_5Si_5O_{20}$), KRb($Ge_5Si_5O_{20}$), KCs($Ge_5Si_5O_{20}$)" nanoclusters with the vibration in the district about "–12 to + 6" Bohr and for the hybrid cluster of "LiRb($Ge_5Si_5O_{20}$)–$2H_2$, LiCs($Ge_5Si_5O_{20}$)–$2H_2$, NaRb($Ge_5Si_5O_{20}$)–$2H_2$, NaCs($Ge_5Si_5O_{20}$)–$2H_2$, KRb($Ge_5Si_5O_{20}$)–$2H_2$, KCs($Ge_5Si_5O_{20}$)–$2H_2$" (Fig. 2a′–f′) in the district about "–12 to + 6" Bohr. Moreover, the elements of "O(2), O(3), O(7)–O(12), O(14), O(15), O(17), O(18), O(22)–O(27), O(29), O(30)" from alkali metal hybrid (Li, Na, K,Rb, Cs)–($Ge_5Si_5O_{20}$) oxide (Fig. 2a–f) have displayed the vibration about "–12 to + 6" Bohr toward construction of hydrogenated alkali metal hybrid (Li, Na, K,Rb, Cs)–($Ge_5Si_5O_{20}$)–$2H_2$ through hydrogen adsorption (Fig. 2a′– f′).

The charge distribution has been illustrated during H-capture by "LiRb ($Ge_5Si_5O_{20}$), LiCs($Ge_5Si_5O_{20}$), NaRb($Ge_5Si_5O_{20}$), NaCs($Ge_5Si_5O_{20}$), KRb($Ge_5Si_5O_{20}$), KCs($Ge_5Si_5O_{20}$)" nanoclusters towards formation of "LiRb($Ge_5Si_5O_{20}$)–$2H_2$, LiCs($Ge_5Si_5O_{20}$)–$2H_2$, NaRb($Ge_5Si_5O_{20}$)–$2H_2$, NaCs($Ge_5Si_5O_{20}$)–$2H_2$, KRb($Ge_5Si_5O_{20}$)–$2H_2$, KCs($Ge_5Si_5O_{20}$)–$2H_2$", respectively (Supplementary Table S1, S2, S3).

Functionalizing of Li, Na, K atoms can augment the negative atomic charge of "O(2), O(3), O(7)–O(12),

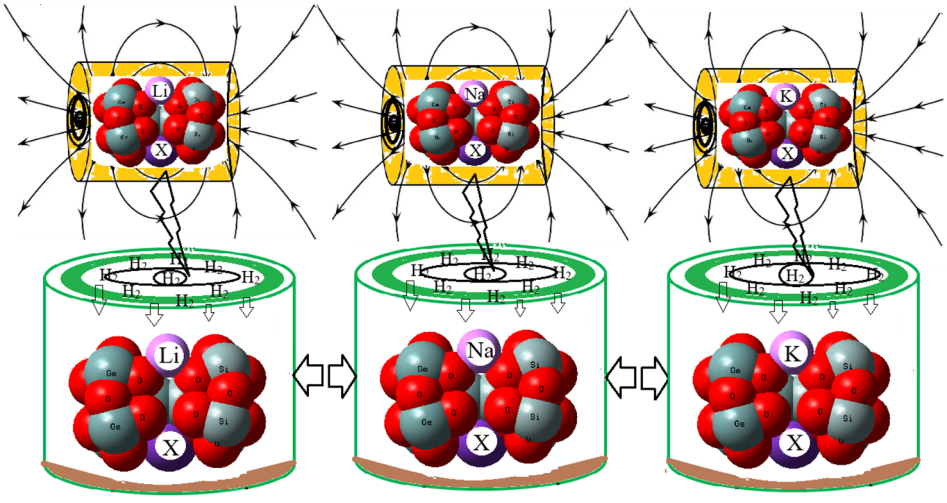

Fig. 1 Adding "Li, Na, K" to ($Ge_5Si_5O_{20}$) nanoclusters accompanying Rb or Cs doping and formation of LiRb ($Ge_5Si_5O_{20}$), LiCs($Ge_5Si_5O_{20}$), NaRb($Ge_5Si_5O_{20}$), NaCs($Ge_5Si_5O_{20}$), KRb($Ge_5Si_5O_{20}$), KCs($Ge_5Si_5O_{20}$) nanoclusters towards energy storage through hydrogen adsorption as LiRb($Ge_5Si_5O_{20}$)–$2H_2$, LiCs($Ge_5Si_5O_{20}$)–$2H_2$, NaRb($Ge_5Si_5O_{20}$)–$2H_2$, NaCs($Ge_5Si_5O_{20}$)–$2H_2$, KRb($Ge_5Si_5O_{20}$)–$2H_2$, KCs($Ge_5Si_5O_{20}$)–$2H_2$ in novel batteries

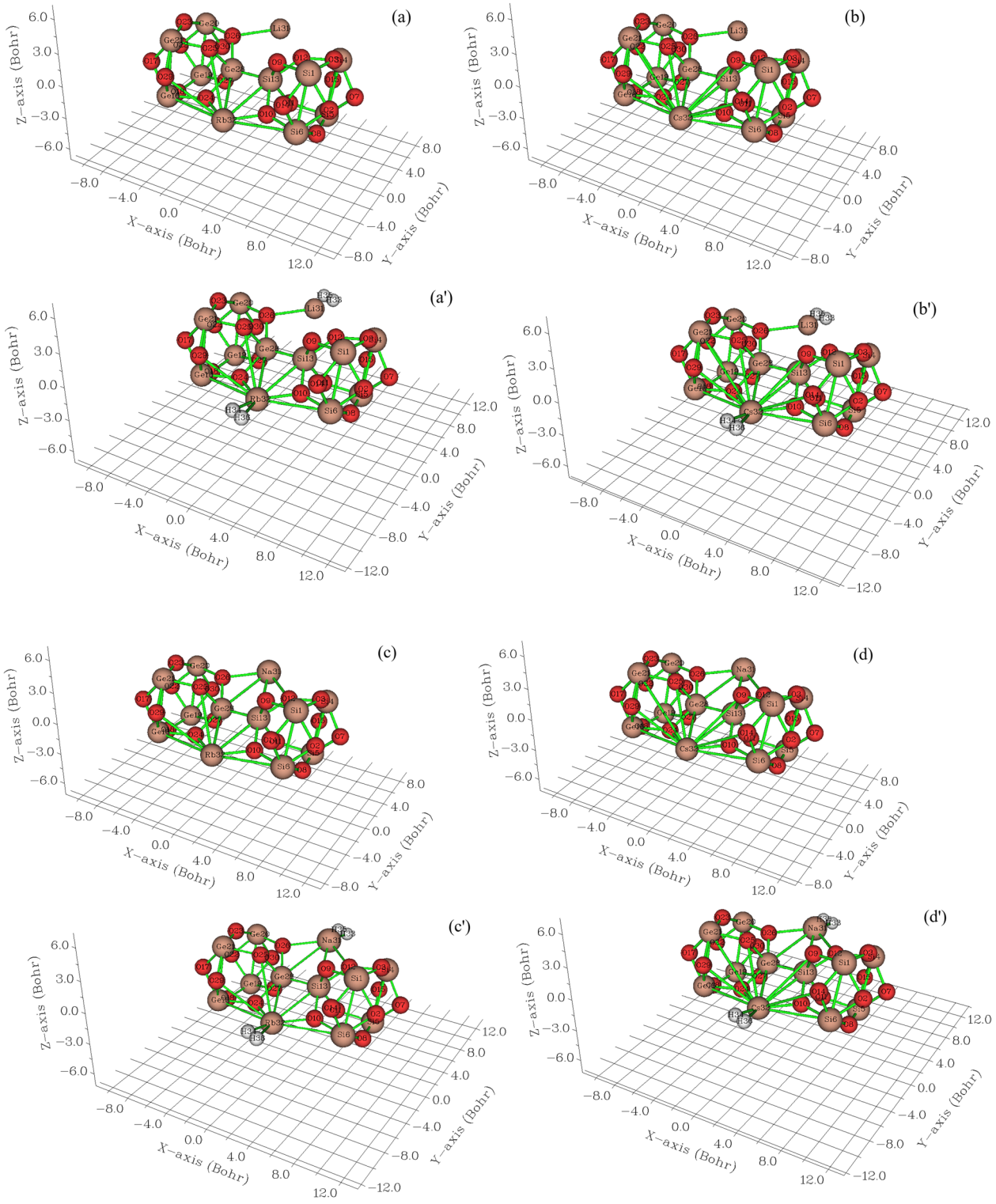

Fig. 2 "CDD graphs" for (**a**) LiRb ($Ge_5Si_5O_{20}$), (**a′**) LiRb($Ge_5Si_5O_{20}$)–$2H_2$, (**b**) LiCs($Ge_5Si_5O_{20}$), (**b′**) LiCs($Ge_5Si_5O_{20}$)–$2H_2$, (**c**) NaRb($Ge_5Si_5O_{20}$), (**c′**) NaRb($Ge_5Si_5O_{20}$)–$2H_2$, (**d**) NaCs($Ge_5Si_5O_{20}$), (**d′**) NaRb($Ge_5Si_5O_{20}$)–$2H_2$, (**e**) KRb($Ge_5Si_5O_{20}$), (**e′**) KRb($Ge_5Si_5O_{20}$)–$2H_2$, (**f**) KCs($Ge_5Si_5O_{20}$), (**f′**) KCs($Ge_5Si_5O_{20}$)–$2H_2$ nanoclusters

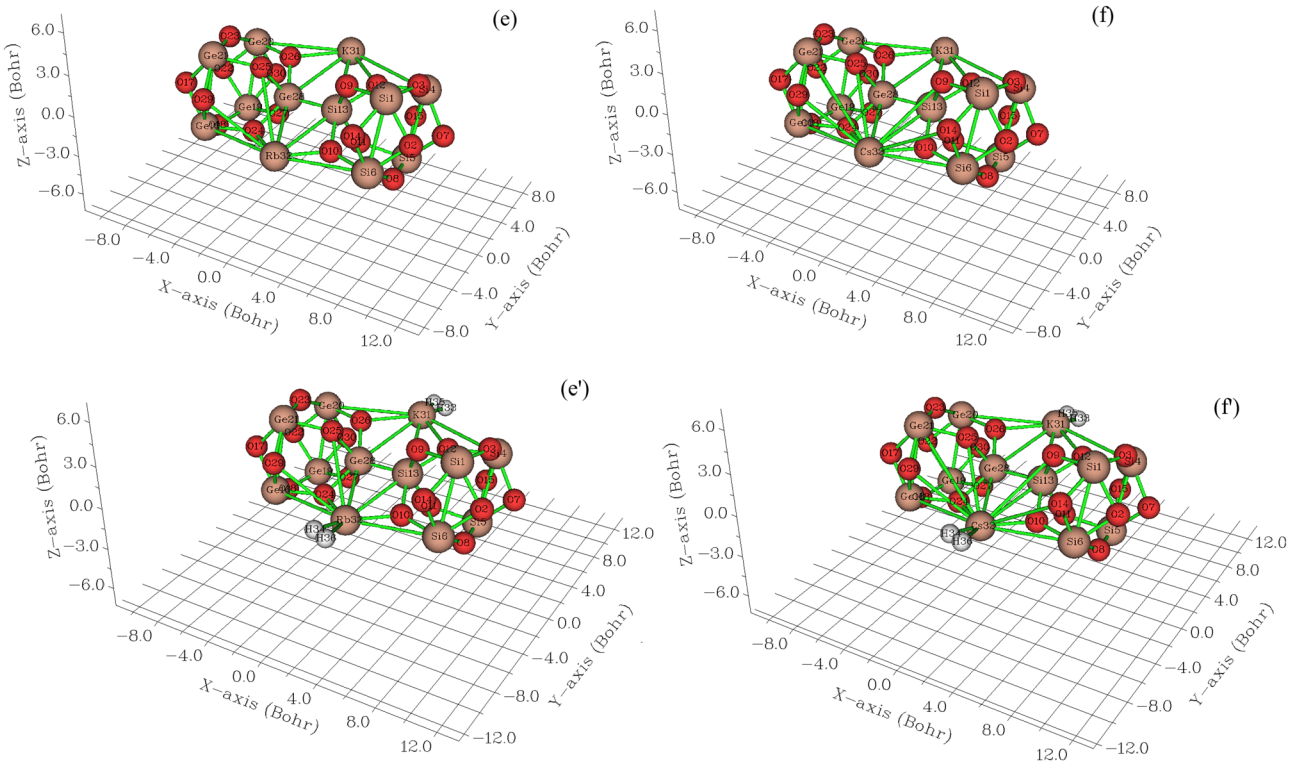

Fig. 2 (continued)

O(14), O(15), O(17), O(18), O(22)–O(27), O(29), O(30)" in "LiRb ($Ge_5Si_5O_{20}$), LiCs($Ge_5Si_5O_{20}$), NaRb($Ge_5Si_5O_{20}$), NaCs($Ge_5Si_5O_{20}$), KRb($Ge_5Si_5O_{20}$), KCs($Ge_5Si_5O_{20}$)" nanoclusters. In fact, "LiRb ($Ge_5Si_5O_{20}$), LiCs($Ge_5Si_5O_{20}$), NaRb($Ge_5Si_5O_{20}$), NaCs($Ge_5Si_5O_{20}$), KRb($Ge_5Si_5O_{20}$), KCs($Ge_5Si_5O_{20}$)" hybrid clusters have displayed more output than ($Ge_5Si_5O_{20}$) for electron acceptance from electron donor of "H(33), H(34), H(35) and H(36)" (Supplementary Table S1, S2, S3).

LiRb ($Ge_5Si_5O_{20}$) and LiCs($Ge_5Si_5O_{20}$) has shown the "Bader charge" of "–1.589 and – 1.552" coulomb before hydrogen adsorption and "–1.591 and – 1.557" coulomb after H_2-capture. Moreover, the flauctuation of charge density values for NaRb($Ge_5Si_5O_{20}$), NaCs($Ge_5Si_5O_{20}$) has shown the "Bader charge" of – 1.580 and – 1.546 C before hydrogen adsorption and – 1.581 and – 1.550 C after hydrogen adsorption. "KRb($Ge_5Si_5O_{20}$) and KCs($Ge_5Si_5O_{20}$)" have shown the "Bader charge" of "–1.555 and – 1.518" coulomb before hydrogen adsorption and "–1.556 and – 1.525" coulomb after H_2-capture.

The differences of charge density value for these hybrid clusters are estimated as: $\Delta Q_{LiRb(Ge5Si5O20)}$ = – 0.002, $\Delta Q_{LiCs(Ge5Si5O20)}$ = – 0.005, $\Delta Q_{NaRb(Ge5Si5O20)}$ = – 0.001, $\Delta Q_{NaCs(Ge5Si5O20)}$ = – 0.004, $\Delta Q_{KRb(Ge5Si5O20)}$ = – 0.001, $\Delta Q_{KCs(Ge5Si5O20)}$ = – 0.007 C. Therefore, the results have shown that the cluster of KCs($Ge_5Si_5O_{20}$), LiCs($Ge_5Si_5O_{20}$) and NaCs($Ge_5Si_5O_{20}$) might have the most gravity for electron receiving owing to H_2-capture.

"Total density of States and overlap projected density of States"

In isolated system (such as molecule), the energy levels are discrete, the concept of "density of state (DOS)" is supposed to be completely valueless in this situation. Therefore, the "original total DOS (TDOS)" of isolated system can be written as [37]:

$$TDOS\ (E) = \sum {}_i\delta\ (E - \epsilon_i) \tag{1}$$

The normalized Gaussian function is defined as:

$$G(x) = \frac{1}{c\sqrt{2\pi}} e^{-\frac{x^2}{2c^2}} \text{where } c = \frac{\text{FWHM}}{2\sqrt{2\ln x}} \tag{2}$$

"FWHM (full width at half maximum)" is an adjustable parameter in "Multiwfn" [38, 39]. Furthermore, the curve map of "broadened partial DOS (PDOS)" and "overlap DOS (OPDOS)" are valuable for visualizing orbital composition analysis, "PDOS function of fragment *A*" is defined as:

$$PDOS_A\ (E) = \sum {}_i\Xi_{i,A}\, F\,(E - \epsilon_i) \tag{3}$$

where" $\Xi_{i,A}$ is the composition of fragment *A* in orbital *i*". The "OPDOS between fragment *A* and *B* "is defined as:

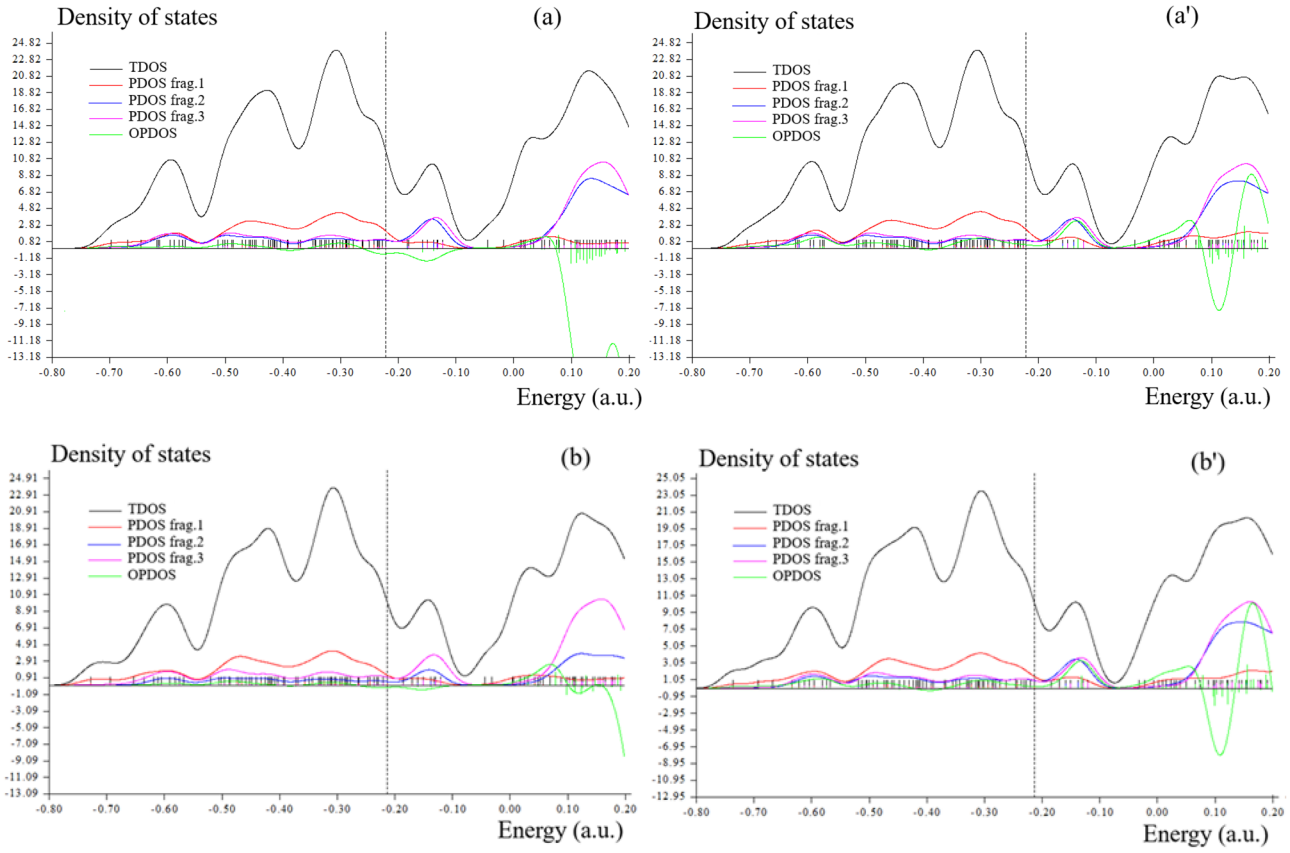

Fig. 3 "TDOS/PDOS/OPDOS graphs" of (**a**) LiRb ($Ge_5Si_5O_{20}$), (**a′**) LiRb($Ge_5Si_5O_{20}$)–$2H_2$, (**b**) LiCs($Ge_5Si_5O_{20}$), (**b′**) LiCs($Ge_5Si_5O_{20}$)–$2H_2$, (**c**) NaRb($Ge_5Si_5O_{20}$), (**c′**) NaRb($Ge_5Si_5O_{20}$)–$2H_2$, (**d**) NaCs($Ge_5Si_5O_{20}$), (**d′**) NaRb($Ge_5Si_5O_{20}$)–$2H_2$, (**e**) KRb($Ge_5Si_5O_{20}$), (**e′**) KRb($Ge_5Si_5O_{20}$)–$2H_2$, (**f**) KCs($Ge_5Si_5O_{20}$), (**f′**) KCs($Ge_5Si_5O_{20}$)–$2H_2$ nanoclusters

$$OPDOS_{A,B}\ (E) = \sum {}_iX^i_{A,B}\ F\ (E - \epsilon_i\ ) \qquad (4)$$

where" $X^i_{A,B}$ is the composition of total cross term between fragment *A* and *B* in orbital *i* ".

In the "TDOS map", each discrete vertical line corresponds to a "molecular orbital (MO)", the dashed line highlights the position of "HOMO". The curve is the "TDOS" simulated based on the distribution of "MO" energy levels.

Regarding adsorption behavior of hydrogen by "LiRb ($Ge_5Si_5O_{20}$), LiCs($Ge_5Si_5O_{20}$), NaRb($Ge_5Si_5O_{20}$), NaCs($Ge_5Si_5O_{20}$), KRb($Ge_5Si_5O_{20}$), KCs($Ge_5Si_5O_{20}$) " nanoclusters, "TDOS" has been evaluated. This factor can demonstrate the existence of important chemical interactions often on the "convex side" (Fig. 3a–f &,a′–f′).

During formation of "LiRb ($Ge_5Si_5O_{20}$), LiCs($Ge_5Si_5O_{20}$), NaRb($Ge_5Si_5O_{20}$), NaCs($Ge_5Si_5O_{20}$), KRb($Ge_5Si_5O_{20}$)" (Fig. 3a, b,c, d,e) and hydrogenated nanoclusters containing "LiRb($Ge_5Si_5O_{20}$)–$2H_2$, LiCs($Ge_5Si_5O_{20}$)–$2H_2$, NaRb($Ge_5Si_5O_{20}$)–$2H_2$, NaCs($Ge_5Si_5O_{20}$)–$2H_2$", KRb($Ge_5Si_5O_{20}$) – $2H_2$ (Fig. 3a′,b′,c′,d′,e′) have shown the steepest maximums surrounding "–0.3, – 0.45 and – 0.60 a.u." owing to covalent bond between two elements of "Li/Rb, Li/Cs, Na/Rb, Na/Cs" with ($Ge_5Si_5O_{20}$) nanocluster.

However, the "TDOS" curve for KCs ($Ge_5Si_5O_{20}$) and KCs ($Ge_5Si_5O_{20}$)–$2H_2$ nanoclusters have shown four pointed peaks around "–0.3, – 0.45, – 0.60, – 0.75 a.u." owing to covalent bond between elements of K and Cs with ($Ge_5Si_5O_{20}$) nanocluster through hydrogen storage with maximum density of state of ≈ 24 surrounding – 0.30 a.u. (Fig. 3f, f′).

Fragment 1 has been defined for O9 to O12, Si13, O24 to O27 and Ge28, X31(X = Li, Na, K)/Y32 (Y = Rb, Cs) in Fig. 3a–f and H36 to H36 in Fig. 3a′–f′. Fragment 2 has indicated the fluctuation of Si1, Si4 to Si6 beside the similar involved atoms of Fragment 1 in Fig. 3a, b, c, d and a′–f′. Finally, it was considered the fluctuation of Ge16, Ge19 to Ge21, O17, O18, O22, O23, O29, O30 in Fig. 3a–f, a′–f′ through Fragment 3.

Localized orbital locator analysis

Trapping of hydrogens by "LiRb ($Ge_5Si_5O_{20}$), LiCs($Ge_5Si_5O_{20}$), NaRb($Ge_5Si_5O_{20}$), NaCs($Ge_5Si_5O_{20}$), KRb($Ge_5Si_5O_{20}$), KCs($Ge_5Si_5O_{20}$)" (Fig. 4a, b,c, d,e, f).nanoclusters towards formation of

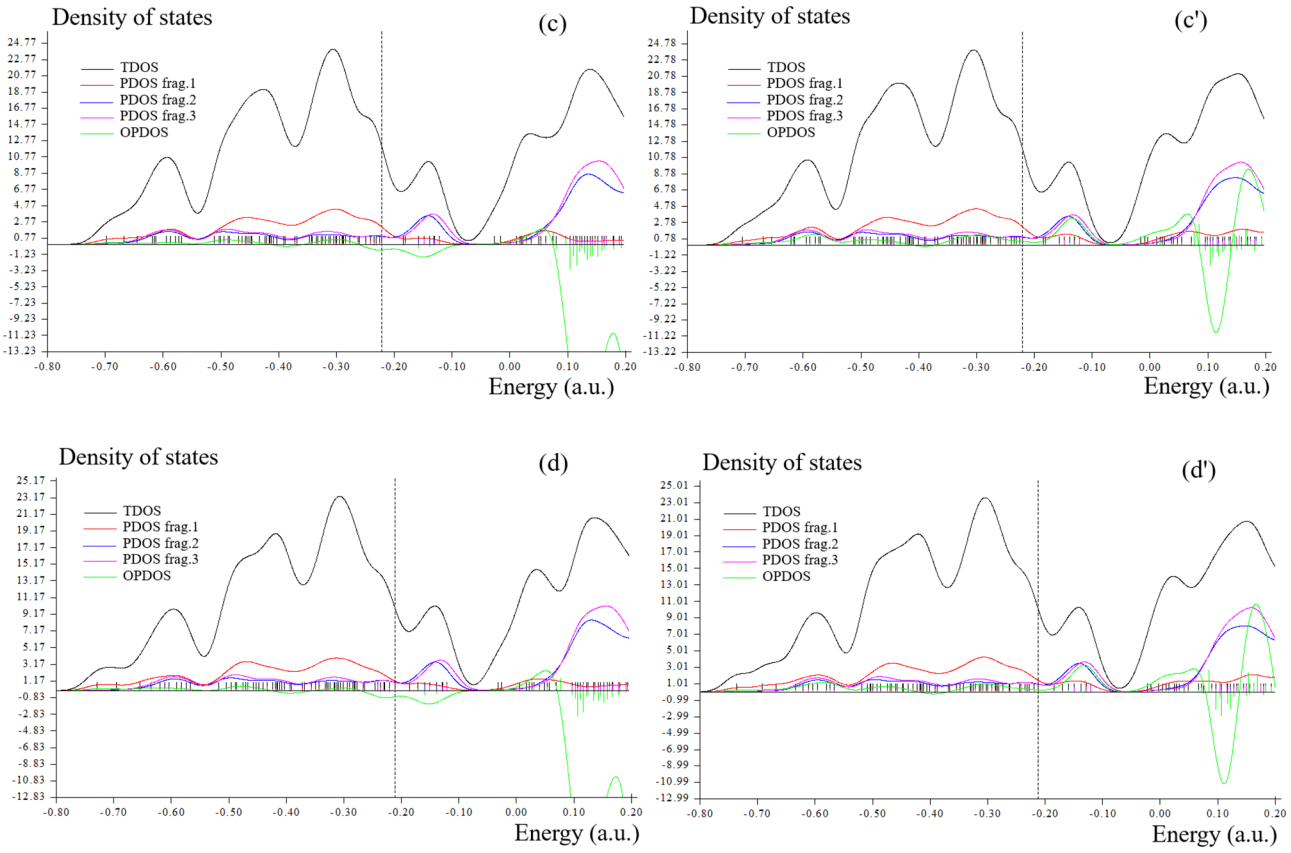

Fig. 3 (continued)

"LiRb($Ge_5Si_5O_{20}$)–$2H_2$, LiCs($Ge_5Si_5O_{20}$)–$2H_2$, NaRb($Ge_5Si_5O_{20}$)–$2H_2$, NaCs($Ge_5Si_5O_{20}$)–$2H_2$, KRb($Ge_5Si_5O_{20}$)–$2H_2$, KCs($Ge_5Si_5O_{20}$)–$2H_2$" might be described by Localized orbital locator (LOL) [40] graphs using "Multiwfn" [38, 39] due to achieving their "delocalization/localization" characterizations [41] of electrons and chemical bonds (Fig. 4a′,b′,c′,d′,e′,f′).

"LiRb ($Ge_5Si_5O_{20}$) (Fig. 4a), LiRb($Ge_5Si_5O_{20}$)–$2H_2$ (Fig. 4a′), LiCs ($Ge_5Si_5O_{20}$) (Fig. 4b), LiCs($Ge_5Si_5O_{20}$)–$2H_2$ (Fig. 4b′), NaRb ($Ge_5Si_5O_{20}$) (Fig. 4c), NaRb($Ge_5Si_5O_{20}$)–$2H_2$ (Fig. 4c′), NaCs ($Ge_5Si_5O_{20}$) (Fig. 4d), NaCs($Ge_5Si_5O_{20}$)–$2H_2$ (Fig. 4d′), KRb ($Ge_5Si_5O_{20}$) (Fig. 4e), KRb($Ge_5Si_5O_{20}$)–$2H_2$ (Fig. 4e′), KCs ($Ge_5Si_5O_{20}$) (Fig. 4f), and KCs($Ge_5Si_5O_{20}$)–$2H_2$" (Fig. 4f′) have demonstarted the electron delocalization through an isosurface map with labeling atoms of "O(10), O(12), Si(13), O(24), O(26), Ge(28), X(31)(X = Li, Na or K), Y(32) (Y = Rb or Cs) and H(33), H(34), H(35), H(36)". In fact, the "counter map of LOL" can confirm that LiRb ($Ge_5Si_5O_{20}$), LiCs($Ge_5Si_5O_{20}$), NaRb($Ge_5Si_5O_{20}$), NaCs($Ge_5Si_5O_{20}$), KRb($Ge_5Si_5O_{20}$), KCs($Ge_5Si_5O_{20}$) nanoclusters may augment the efficiency during H_2-capture towards formation of LiRb($Ge_5Si_5O_{20}$)–$2H_2$, LiCs($Ge_5Si_5O_{20}$)–$2H_2$, NaRb($Ge_5Si_5O_{20}$)–$2H_2$, NaCs($Ge_5Si_5O_{20}$)–$2H_2$, KRb($Ge_5Si_5O_{20}$)–$2H_2$, KCs($Ge_5Si_5O_{20}$)–$2H_2$.

Besides, "intermolecular orbital overlap integral" is important in illustration of intermolecular charge transfer which can compute "HOMO-HOMO" and "LUMO-LUMO" overlap integrals between the H_2 molecules and heteroclusters of LiRb($Ge_5Si_5O_{20}$), LiRb($Ge_5Si_5O_{20}$)–$2H_2$, LiCs($Ge_5Si_5O_{20}$), LiCs($Ge_5Si_5O_{20}$)–$2H_2$, NaRb($Ge_5Si_5O_{20}$), NaRb($Ge_5Si_5O_{20}$) – $2H_2$, NaCs($Ge_5Si_5O_{20}$), NaCs($Ge_5Si_5O_{20}$)–$2H_2$, KRb($Ge_5Si_5O_{20}$), KRb($Ge_5Si_5O_{20}$)–$2H_2$, KCs($Ge_5Si_5O_{20}$), and KCs($Ge_5Si_5O_{20}$)–$2H_2$ nanoclusters. The layered germanium-silicon oxide improved by alkali metal lithium doping have indicated the structural stability of Li-, Na-, K-ion batteries through the reported stability energy in Supplementary Table S4.

A small portion of Rb or Cs entered the Ge–Si layer to replace the Li, Na or K sites might improve the structural stability of the electrode material at high multiplicity, thereby improving the capacity retention rate of 58.5209, 55.6390, 57.5131, 54.7273, 56.5360, 53.8418 for LiRb($Ge_5Si_5O_{20}$), LiCs($Ge_5Si_5O_{20}$), NaRb($Ge_5Si_5O_{20}$), NaCs($Ge_5Si_5O_{20}$), KRb($Ge_5Si_5O_{20}$), KCs($Ge_5Si_5O_{20}$) mAh g^{-1}, respectively (Table S4). Furthermore, the binding energies of hydrogen adsorption by LiRb($Ge_5Si_5O_{20}$), LiCs($Ge_5Si_5O_{20}$), NaRb($Ge_5Si_5O_{20}$), NaCs($Ge_5Si_5O_{20}$), KRb($Ge_5Si_5O_{20}$), KCs($Ge_5Si_5O_{20}$) have been achieved as

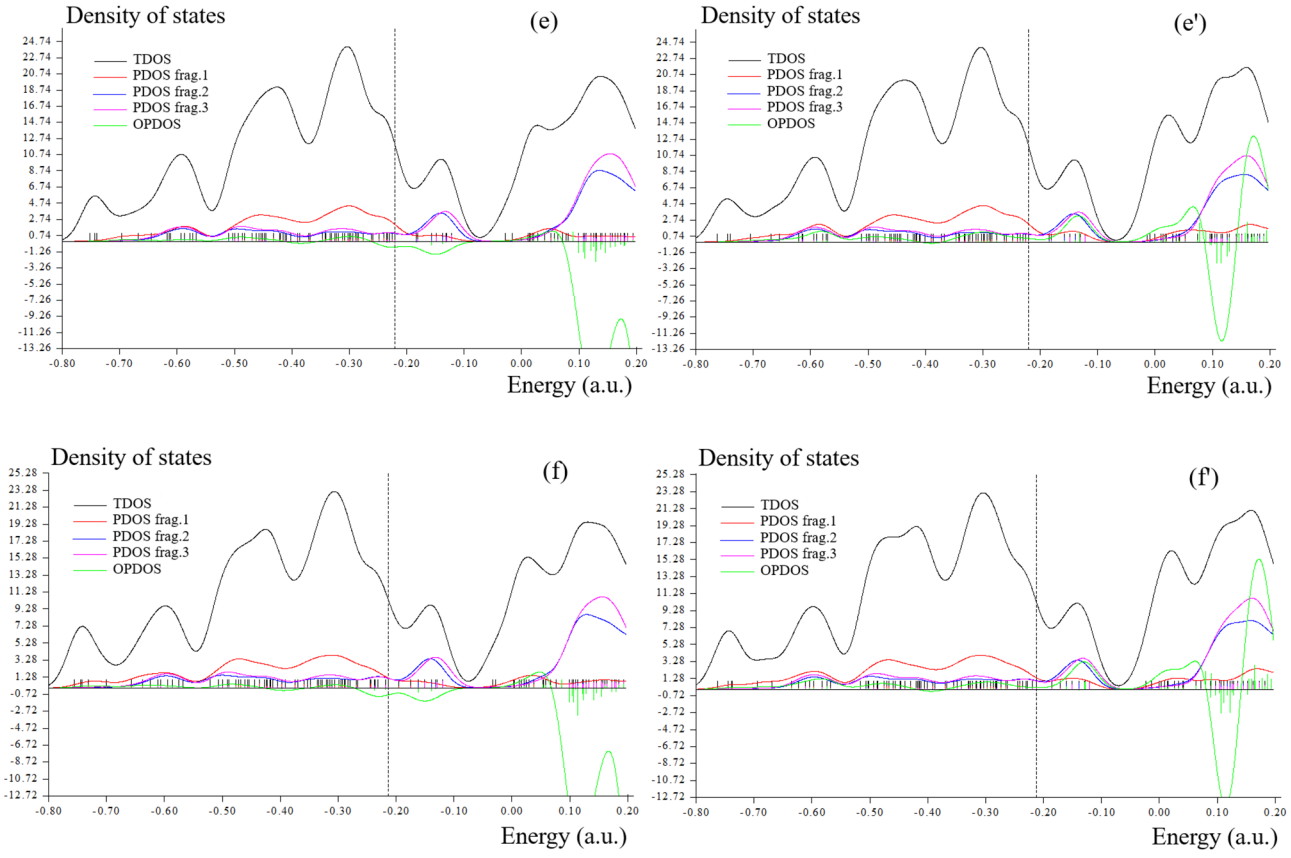

Fig. 3 (continued)

-1.4284, -1.4042, -1.4234, -1.4008, -1.4107, -1.3898 kcal/mol, respectively. The results of cell capacity and binding energy in Table S4 have indicated that LiRb($Ge_5Si_5O_{20}$), NaRb($Ge_5Si_5O_{20}$) KRb($Ge_5Si_5O_{20}$) nanoclusters have more intension for hydrogen adsorption.

As it is seen in Supplementary Table S4, KRb($Ge_5Si_5O_{20}$), KRb($Ge_5Si_5O_{20}$)–$2H_2$, KCs($Ge_5Si_5O_{20}$), and KCs($Ge_5Si_5O_{20}$)–$2H_2$ heteroclusters have shown more stability than LiRb($Ge_5Si_5O_{20}$), LiRb($Ge_5Si_5O_{20}$)–$2H_2$, LiCs($Ge_5Si_5O_{20}$), LiCs($Ge_5Si_5O_{20}$)–$2H_2$, NaRb($Ge_5Si_5O_{20}$), NaRb($Ge_5Si_5O_{20}$) – $2H_2$, NaCs($Ge_5Si_5O_{20}$), NaCs($Ge_5Si_5O_{20}$)–$2H_2$ heteroclusters through the evaluation of stability energy (Es) (Fig. 5).

In this research, hydrogen energy sources on functionalized 2D materials by metals have been shown as promising alternatives for clean energy systems. In a particular way, we have demonstrated here that ($Ge_5Si_5O_{20}$) weakly adsorbs H_2. At the same time, the Li/Na/K decoration significantly enhances the H_2 interaction, accommodating to H_2 molecules by a stronger physisorption. Also, scanning bond orders confirm a great interaction between the LiRb ($Ge_5Si_5O_{20}$), LiCs($Ge_5Si_5O_{20}$), NaRb($Ge_5Si_5O_{20}$), NaCs($Ge_5Si_5O_{20}$), KRb($Ge_5Si_5O_{20}$), KCs($Ge_5Si_5O_{20}$) systems and the hydrogen, a distinct scenario for the pristine ($Ge_5Si_5O_{20}$).

Conclusions

H_2-capture by the nanoclusters of "LiRb ($Ge_5Si_5O_{20}$), LiCs($Ge_5Si_5O_{20}$), NaRb($Ge_5Si_5O_{20}$), NaCs($Ge_5Si_5O_{20}$), KRb($Ge_5Si_5O_{20}$), KCs($Ge_5Si_5O_{20}$)" was studied by computational method". The changes of charge density defined a notable charge transfer in "LiRb ($Ge_5Si_5O_{20}$), LiCs($Ge_5Si_5O_{20}$), NaRb($Ge_5Si_5O_{20}$), NaCs($Ge_5Si_5O_{20}$), KRb($Ge_5Si_5O_{20}$), KCs($Ge_5Si_5O_{20}$)". Besides, thermodynamic parameters describing H_2-capture by alkali metals hybrid clusters of "LiRb ($Ge_5Si_5O_{20}$), LiCs($Ge_5Si_5O_{20}$), NaRb($Ge_5Si_5O_{20}$), NaCs($Ge_5Si_5O_{20}$), KRb($Ge_5Si_5O_{20}$), KCs($Ge_5Si_5O_{20}$)" have been studied consisting of internal process of the "adsorbent–adsorbate" process. It is well established that enhancing of Li, Na or K to cell batteries might augment the energy-saving in cell batteries. Therefore, it has been discovered the influence of "Rb- or Cs-doped Li-, Na-, K-ion" batteries. Moreover, "hydrogen bond (H-bond)" accepting sites by "LiRb ($Ge_5Si_5O_{20}$), LiCs($Ge_5Si_5O_{20}$), NaRb($Ge_5Si_5O_{20}$), NaCs($Ge_5Si_5O_{20}$), KRb($Ge_5Si_5O_{20}$), KCs($Ge_5Si_5O_{20}$)" can alleviate "parasitic hydrogen evolution" in H_2O-electrolytes in Li-, Na-, K-ion batteries. The results of this research article represent that the architectural design of "XY($Ge_5Si_5O_{20}$) (X = Li, Na, K/Y = Rb, Cs)" can augment the capacity of battery cell. This research article is useful for designing

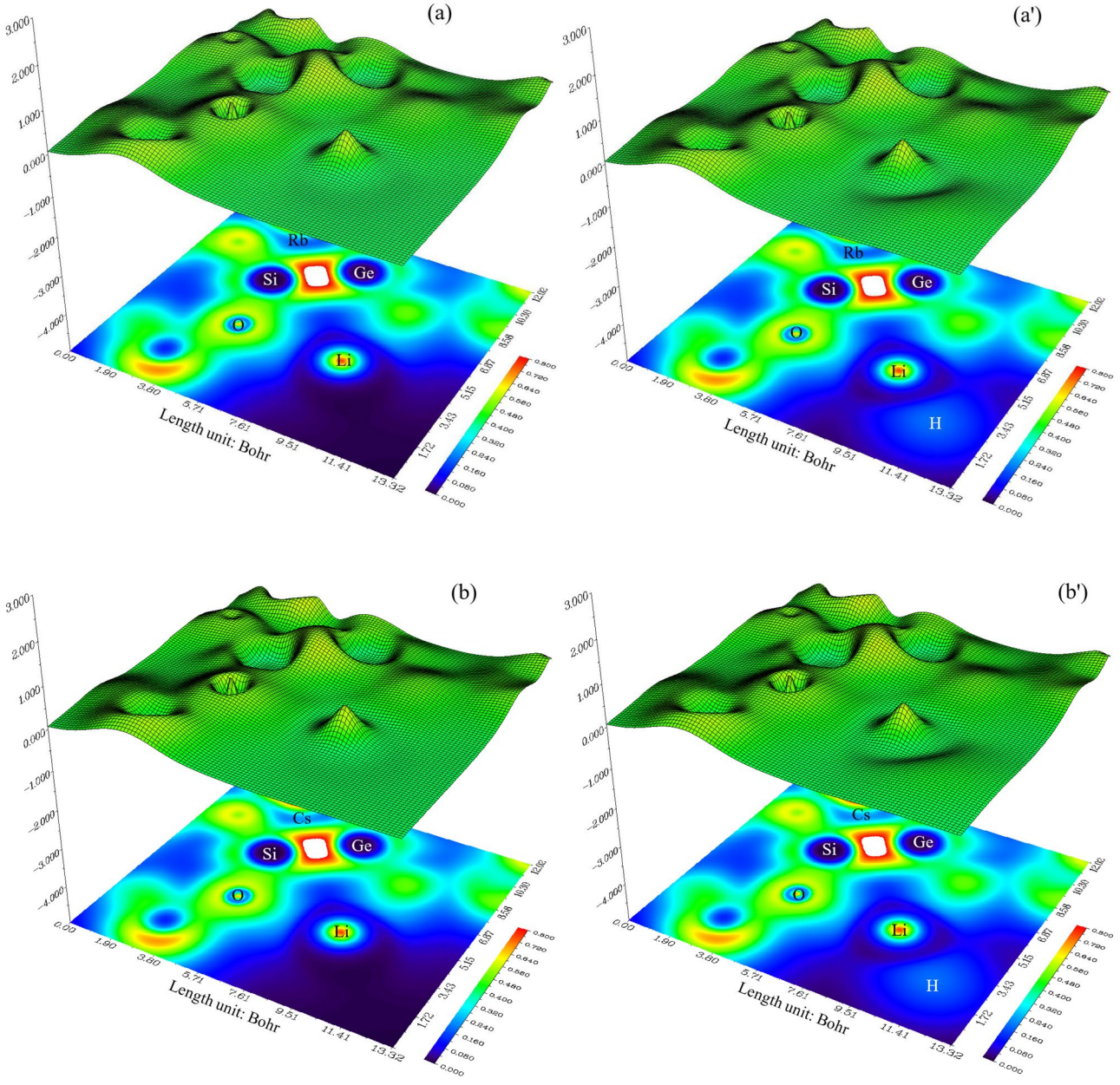

Fig. 4 The "counter map of LOL graphs" for (**a**) LiRb ($Ge_5Si_5O_{20}$), (**a′**) LiRb($Ge_5Si_5O_{20}$)–$2H_2$, (**b**) LiCs($Ge_5Si_5O_{20}$), (**b′**) LiCs($Ge_5Si_5O_{20}$)–$2H_2$, (**c**) NaRb($Ge_5Si_5O_{20}$), (**c′**) NaRb($Ge_5Si_5O_{20}$)–$2H_2$, (**d**) NaCs($Ge_5Si_5O_{20}$), (**d′**) NaRb($Ge_5Si_5O_{20}$)–$2H_2$, (**e**) KRb($Ge_5Si_5O_{20}$), (**e′**) KRb($Ge_5Si_5O_{20}$)–$2H_2$, (**f**) KCs($Ge_5Si_5O_{20}$), (**f′**) KCs($Ge_5Si_5O_{20}$)–$2H_2$ nanoclusters

and constructing of alkali metals hybrid batteries (Li/Na/K, Rb/Cs)with high power density/energy with excellent cycle stability, and will represent a perspective for the industrial application of alkali metals hybrid batteries. Recent study have shown that two-dimensional (2D) SiGe-based materials as electrode in alkali metals batteries can lead to excellent enery storage.

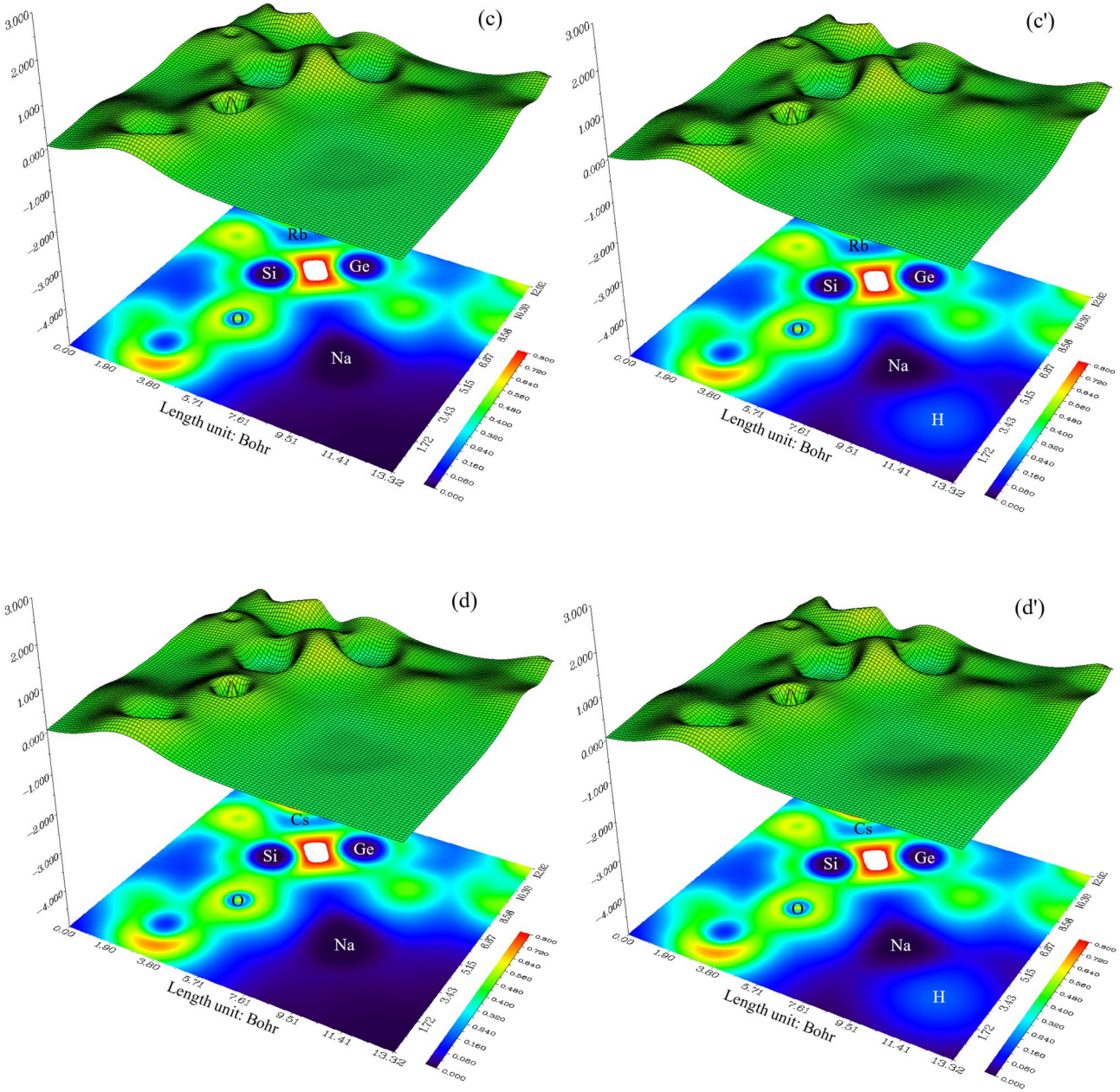

Fig. 4 (continued)

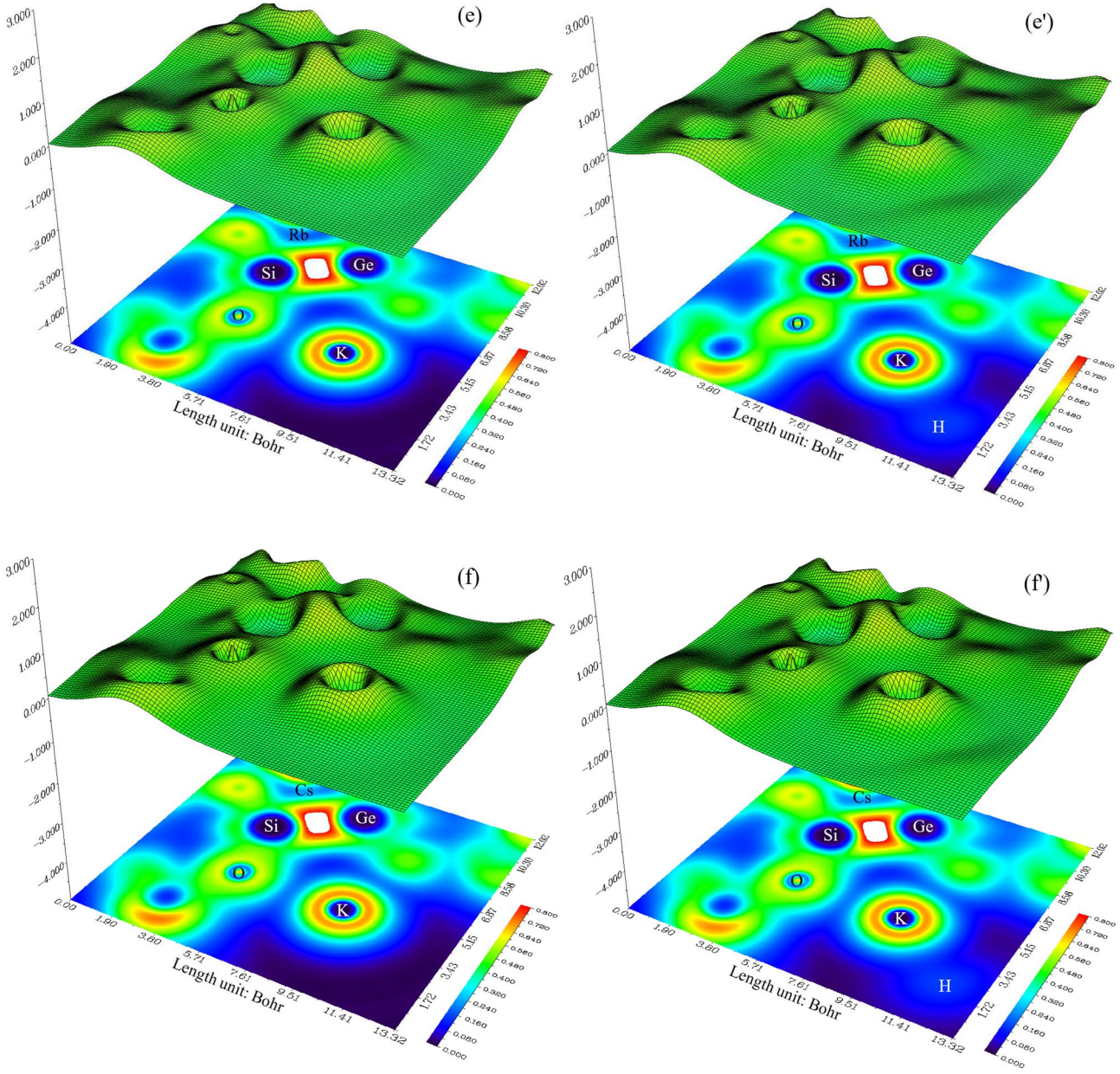

Fig. 4 (continued)

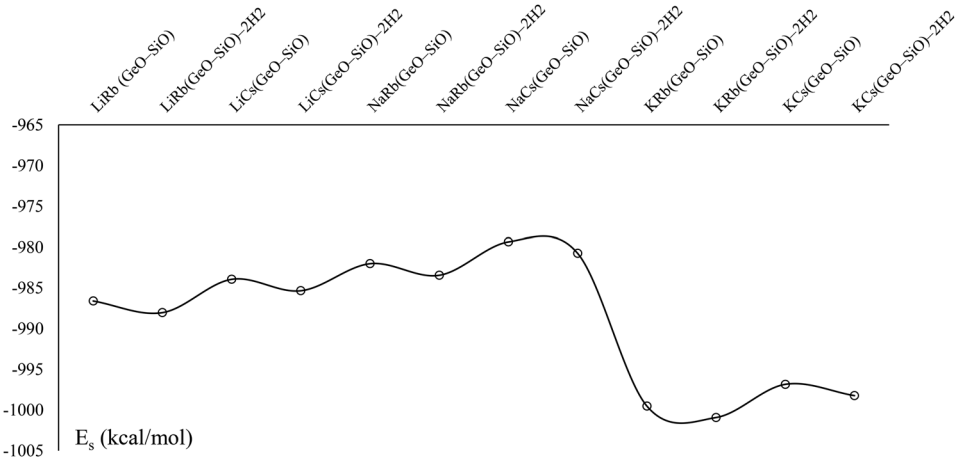

Fig. 5 The stability energy (E_s) (kcal/mol) for LiRb ($Ge_5Si_5O_{20}$), LiRb($Ge_5Si_5O_{20}$)–$2H_2$, LiCs($Ge_5Si_5O_{20}$), LiCs($Ge_5Si_5O_{20}$)–$2H_2$, NaRb($Ge_5Si_5O_{20}$), NaRb($Ge_5Si_5O_{20}$)–$2H_2$, NaCs($Ge_5Si_5O_{20}$), NaRb($Ge_5Si_5O_{20}$)–$2H_2$, KRb($Ge_5Si_5O_{20}$), KRb($Ge_5Si_5O_{20}$)–$2H_2$, KCs($Ge_5Si_5O_{20}$), KCs($Ge_5Si_5O_{20}$)–$2H_2$ heteroclusters

Supplementary Information

The online version contains supplementary material available at https://doi.org/10.1186/s13065-025-01593-0.

Supplementary Material 1

Acknowledgements
The author is grateful to Kastamonu University for completing this paper and its research.

Author contributions
FM analyzed and interpreted the nanostructures data regarding charge density differences, total density of states, and electron localization function. She performed the theoretical calculations, and she was the only contributor in writing, reading and approving the final manuscript.

Funding
This research received no external funding.

Data availability
No datasets were generated or analysed during the current study.

Declarations

Ethical approval
Not applicable.

Consent to participate
Not applicable.

Consent for publication
Not applicable.

Competing interests
The authors declare no competing interests.

Received: 26 February 2025 / Accepted: 21 July 2025
Published online: 06 August 2025

References

1. Yang H, Wu Nl. Conductivity and ion transport mechanisms of Solid-State Lithium-Ion battery electrolytes: A review. Energy Sci Eng. 2022;10:1643–71.
2. Walvekar H, Beltran H, Sripad S, Pecht M. Implications of the electric vehicle manufacturers' decision to mass adopt Lithium-Iron phosphate batteries. IEEE Access. 2022;10:63834–43.
3. Choi D, Shamim N, Crawford A, Huang Q, Vartanian CK, Viswanathan VV, Paiss MD, Alam MJE, Reed DM, Sprenkle VL. Li-Ion battery technology for grid application. J Power Sources. 2021;511:230419.
4. Ahmad T, Zhang DA, Critical. Review of comparative global historical energy consumption and future demand: the story told so Far. Energy Rep. 2020;6:1973–91.
5. Mlilo N, Brown J, Ahfock T. Impact of intermittent renewable energy generation penetration on the power system Networks—A review. Technol Econ Smart Grids Sustain Energy. 2021;6:25.
6. Rautela R, Yadav BR, Kumar SA. Review on technologies for recovery of metals from waste Lithium-Ion batteries. J Power Sources. 2023;580:233428.
7. Tan AKX, Paul S. Beyond lithium: future battery technologies for sustainable energy storage. Energies. 2024;17:5768. https://doi.org/10.3390/en17225768.
8. Singh AN, Islam M, Meena A, Faizan M, Han D, Bathula C, Hajibabaei A, Anand R, Nam KW. Unleashing the potential of Sodium-Ion batteries: current state and future directions for sustainable energy storage. Adv Funct Mater. 2023;33:2304617.
9. Gu ZY, Guo JZ, Cao JM, Wang XT, Zhao XX, Zheng XY, Li WH, Sun ZH, Liang HJ, Wu XL. An advanced High-Entropy fluorophosphate cathode for Sodium-Ion batteries with increased working voltage and energy density. Adv Mater. 2022;34:2110108.
10. Jin Y, Le PML, Gao P, Xu Y, Xiao B, Engelhard MH, Cao X, Vo TD, Hu J, Zhong L, et al. Low-Solvation electrolytes for High-Voltage Sodium-Ion batteries. Nat Energy. 2022;7:718–25.
11. Zhang X, Xiong T, He B, Feng S, Wang X, Wei L, Mai L. Recent advances and perspectives in aqueous Potassium-Ion batteries. Energy Environ Sci. 2022;15:3750–74.
12. Ge J, Fan L, Rao AM, Zhou J, Lu B. Surface-Substituted Prussian blue analogue cathode for sustainable Potassium-Ion batteries. Nat Sustain. 2022;5:225–34.
13. Ji B, Yao W, Zheng Y, Kidkhunthod P, Zhou X, Tunmee S, Sattayaporn S, Cheng HM, He H, Tang Y. A fluoroxalate cathode material for Potassium-Ion batteries with Ultra-Long cyclability. Nat Commun. 2020;11:1225.
14. Nazeer W, Farooq A, Younas M, Munir M, Kang SM. On molecular descriptors of carbon nanocones. Biomolecules. 2018;8(92). https://doi.org/10.3390/biom8030092.
15. Zhao J, Li Z, Cole MT, Wang A, Guo X, Liu X, Lyu W, Teng H, Qv Y, Liu G, et al. Nanocone-Shaped carbon nanotubes Field-Emitter array fabricated by laser ablation. Nanomaterials. 2021;11:3244. https://doi.org/10.3390/nano11123244.
16. Mollaamin F. Possibility of the application of Si_5O_{10}–Ge_5O_{10} for increasing H-adsorption towards the energy storage in transistors rather than Li-ion batteries. Clean Energy Sci Technol. 2025;3(1):286. https://doi.org/10.18686/cest286.
17. Nuttapon Yodsin H, Sakagami T, Udagawa T, Ishimoto S, Jungsuttiwong M, Tachikawa. Metal-doped carbon nanocones as highly efficient catalysts for hydrogen storage: nuclear quantum effect on hydrogen spillover

mechanism. Mol Catal. 2021;504:111486. https://doi.org/10.1016/j.mcat.2021.111486.
18. Taha HO, Mahdy AME, Shemy FESE, Hassan MM. Hydrogen storage in sic, gec, and SnC nanocones functionalized with nickel, density functional Theory—Study. Int J Uantum Chem. 2023;123(3):e27023. https://doi.org/10.1002/qua.27023.
19. Wei T, Zhou Y, Sun C, et al. An intermittent lithium deposition model based on CuMn-bimetallic MOF derivatives for composite lithium anode with ultrahigh areal capacity and current densities. Nano Res. 2023. https://doi.org/10.1007/s12274-023-6187-8.
20. Mollaamin F, Monajjemi M. Nanomaterials for sustainable energy in Hydrogen-Fuel cell: functionalization and characterization of carbon Nano-Semiconductors with silicon, germanium, Tin or lead through density functional theory study. Russ J Phys Chem B. 2024;18:607–23. https://doi.org/10.1134/S1990793124020271.
21. Mollaamin F, Shahriari S, Monajjemi M. Influence of transition metals for emergence of energy storage in fuel cells through hydrogen adsorption on the MgAl surface. Russ J Phys Chem B. 2024;18:398–418. https://doi.org/10.1134/S199079312402026X.
22. Mollaamin F. Features of parametric point nuclear magnetic resonance of metals implantation on Boron nitride nanotube by density functional theory/electron paramagnetic resonance. J Comput Theor Nanosci. 2014;11:2393–8.
23. Haiying Che J, Liu H, Wang X, Wang, Sheng S, Zhang X-Z, Liao Z-F, Ma. Rubidium and cesium ions as electrolyte additive for improving performance of hard carbon anode in sodium-ion battery. Electrochem Commun. 2017;83:20–3. https://doi.org/10.1016/j.elecom.2017.08.012.
24. Masood MK, Wang J, Song J, Liu Y. Exploring the potential of MB_4 (M = Cr, mo, and W) MBenes as high-capacity anode materials for Ca-ion batteries: a DFT approach. J Mater Chem A. 2024;1222945–59. https://doi.org/10.1039/D4TA02176B.
25. Masood MK, Wang J, Song J, Liu Y. A novel two-dimensional whorled CrB4 and MoB4 as high-performance anode material for metal ion batteries. Appl Surf Sci. 2024;652:159301. https://doi.org/10.1016/j.apsusc.2024.159301.
26. Russell NM, Ekerdt JG. Kinetics of hydrogen desorption from germanium-covered Si(100). Surf Sci. 1996;369(3):1. https://doi.org/10.1016/S0039-6028(96)00888-6.
27. Tok ES, Ong SW, Chuan H, Kang. Hydrogen desorption kinetics from the $Si_{(1-x)}Ge_x$(100)-(2×1) surface. J Chem Phys. 2004;120:5424–31. https://doi.org/10.1063/1.1645510.
28. Grimme S, Ehrlich S, Goerigk L. Effect of the damping function in dispersion corrected density functional theory. J Comput Chem. 2011;32:1456–65. https://doi.org/10.1002/jcc.21759.
29. Henkelman G, Arnaldsson A, Jónsson H. A fast and robust algorithm for bader decomposition of charge density. Comput Mater Sci. 2006;36(3):354–60.
30. Mollaamin F, Monajjemi M. Adsorption ability of Ga_5N_{10} nanomaterial for removing metal ions contamination from drinking water by DFT. Int J Quantum Chem. 2024;124:e27348. https://doi.org/10.1002/qua.27348.
31. Mollaamin F, Monajjemi M. Molecular modelling framework of metal-organic clusters for conserving surfaces: Langmuir sorption through the TD-DFT/ONIOM approach. Mol Simul. 2023;49(4):365–76. https://doi.org/10.1080/08927022.2022.2159996.
32. Mollaamin F. Competitive intracellular Hydrogen-Nanocarrier among aluminum, carbon, or silicon implantation: a novel technology of Eco-Friendly energy storage using research density functional theory. Russ J Phys Chem B. 2024;18:805–20. https://doi.org/10.1134/S1990793124700131.
33. Masood MK, Chaoui K, Rehman J, Khan W, Ashraf IU, Hassan H. Aboud Ahmed Awadh bahajjaj, exploring the potential of two-dimensional MB4 (M = Cr, mo, and W) monolayer as a high-capacity negative electrode material for Al-ion batteries. Surf Interfaces. 2024;54:105254. https://doi.org/10.1016/j.surfin.2024.105254.
34. Frisch MJ, Trucks GW, Schlegel HB, Scuseria GE, Robb MA et al. Gaussian 16, Revision C.01, Gaussian, Inc., Wallingford CT, 2016.
35. GaussView, Keith R, Millam TA. John M. Semichem Inc., Shawnee Mission, KS, 2016.
36. Xu Z, Qin C, Yu Y, Jiang G, Zhao L. First-principles study of adsorption, dissociation, and diffusion of hydrogen on α-U (110) surface. AIP Adv. 2024;14:055114. https://doi.org/10.1063/5.0208082.
37. Becke AD, Edgecombe KE. J Chem Phys. 1990;9:5397–403. https://doi.org/10.1063/1.458517.
38. Tian Lu F, Chen. Multiwfn: A multifunctional wavefunction analyzer. J Comput Chem. 2012;33:580–92. https://doi.org/10.1002/jcc.22885.
39. Tian, Lu. A comprehensive electron wavefunction analysis toolbox for chemists. Multiwfn J Chem Phys. 2024;161:082503. https://doi.org/10.1063/5.0216272.
40. Schmider HL, Becke AD. Chemical content of kinetic energy density. J Mol Struct (Thoechem). 2000;527(1–3):51–61. https://doi.org/10.1016/S0166-1280(00)00477-2.
41. Tsirelson V, Stash A. Analyzing experimental electron density with the localized-orbital locator. Acta Cryst B. 2002;58:780–5. https://doi.org/10.1107/S0108768102012338.

Publisher's note